PHOTORESISTORS

A photoresistor detector (also called a photoconductor) is essentially a radiation-sensitive resistor. In this device the radiation changes the electrical conductivity of the material upon which it is incident. The change in conductivity is measured by means of electrodes attached to the sample. The sample geometry and circuit employed for detecting the photoconduc-

J. Webster (ed.), *Wiley Encyclopedia of Electrical and Electronics Engineering*. Copyright © 1999 John Wiley & Sons, Inc.

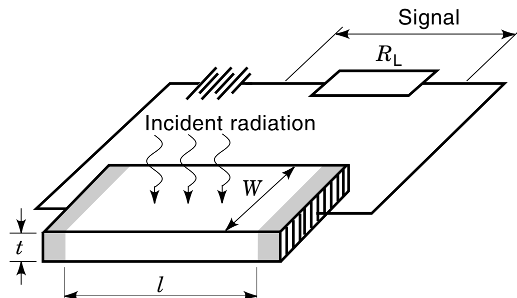

Figure 1. Geometry and bias of a photoresistor.

tive effect is shown in Fig. 1. In almost all cases the transverse geometry is used, in which the direction of the incident radiation is perpendicular to the direction in which the change in current is measured. The photosignal is detected either as a change in voltage developed across a load resistor in series with the detector as illustrated, or as a change in current through the sample. For low-resistance material, the photoresistor is usually operated in a constant current circuit as showed in Fig. 1. The series load resistance is large compared to the sample resistance, and the signal is detected as a change in voltage developed across the sample. For high-resistance photoconductors, a constant-voltage circuit is preferred and the signal is detected as a change in current in the bias circuit.

Figure 2 illustrates the three fundamental optical excitation processes that can occur in semiconductors. Intrinsic band-to-band absorption occurs [Fig. 2(a)] when the photon energy is greater than the material bandgap energy E_g, and a photon is able to excite an electron from the valence band up into the conduction band. The hole and electron each constitute a charge carrier. The application of an electric field to the semiconductor causes the hole and electron to be transported through the material and into the external circuit, causing a photocurrent to flow. The long wavelength limit of an intrinsic photoresistor is

$$\lambda_c = \frac{hc}{E_g} \quad \text{or} \quad \lambda_c[\mu\text{m}] = \frac{1.24}{E_g[\text{eV}]} \qquad (1)$$

where h is Planck's constant and c is the speed of light.

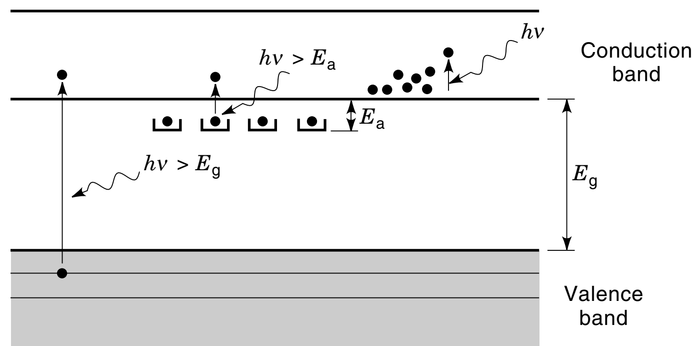

Figure 2. Fundamental optical excitation processes in semiconductors: intrinsic absorption, extrinsic absorption, free carrier absorption.

Extrinsic photoconductivity occurs when an incident photon, lacking sufficient energy to produce a free hole–electron pair, becomes excitated at an impurity center in the form of either a free electron-bound hole or a free hole-bound electron, which is shown in Fig. 2(b). The long wavelength limit of an extrinsic photoeffect is thus given by

$$\lambda_c = \frac{hc}{E_i} \quad \text{or} \quad \lambda_c[\mu\text{m}] = \frac{1.24}{E_i[\text{eV}]} \qquad (2)$$

where E_i is the impurity ionization energy. Band-to-impurity absorption is used in the very long wavelength infrared region to construct photoresistors responsible at wavelengths as long as 30 μm.

Free-carrier absorption is a secondary effect used for very long wavelength infrared regions. Radiation falling on a high-mobility semiconductor (such as InSb) induces intraband transitions and increases the mean energy of the conduction electrons. Since the carrier mobility is a function of the electron temperature, a change in conductivity may be observed. The device is usually operated at very low temperatures, near 4 K, to reduce the rate of energy transfer to the lattice.

The performance of a photoresistor is measured in terms of the following parameters: current (or voltage) responsivity, photoconductive gain, detectivity, and response time.

CURRENT AND VOLTAGE RESPONSIVITY

We assume that the signal photon flux density $\Phi_s(\lambda)$ is incident on the detector area $A = wl$ and that the detector is operated under constant current conditions, that is, $R_L \gg R$. We suppose further that the illumination and the bias field are weak, and the excess carrier lifetime, τ, is the same for majority and minority carriers. To derive an expression for voltage responsivity, we take a one-dimensional approach for simplicity. This is justified for a detector thickness, t, which is small with respect to the minority carrier diffusion length. We also neglect the effect of recombination at frontal and rear surfaces.

The basic expression describing photoconductivity in semiconductors under equilibrium excitation (i.e., steady state) is

$$I_{ph} = q\eta A\Phi_s g \qquad (3)$$

where I_{ph} is the short-circuit photocurrent at zero frequency [direct current (dc)]—that is, the increase in current above the dark current accompanying irradiation. The quantum efficiency, η, describes how well the detector is coupled to the radiation to be detected. It is defined as the number of excess carriers generated per incident photon. The photoconductive gain, g, is the number of carriers passing contacts per one generated pair.

In general, photoconductivity is a two-carrier phenomenon, and the total photocurrent of electrons and holes is

$$I_{ph} = \frac{wtq(\Delta n\mu_e + \Delta p\mu_h)V_b}{l} \qquad (4)$$

where μ_e is the electron mobility, μ_h is the hole mobility, V_b is the bias voltage, and

$$n = n_0 + \Delta n, \qquad p = p_0 + \Delta p \qquad (5)$$

where n_0 and p_0 are the average thermal equilibrium carrier densities, and Δn and Δp are the excess carrier concentrations.

Taking the conductivity to be dominated by electrons (in all known high-sensitivity photoconductors, this is found to be the case) and assuming uniform and complete absorption of the light in the detector, the rate equation for the excess electron concentration in the sample is

$$\frac{d\Delta n}{dt} = \frac{\Phi_s \eta}{\mathrm{t}} - \frac{\Delta n}{\tau} \tag{6}$$

where τ is the excess carrier lifetime (1). In the steady condition, the excess carrier lifetime is given by the equation

$$\tau = \frac{\Delta n t}{\eta \Phi_s} \tag{7}$$

Equating Eq. (3) with Eq. (4) gives

$$g = \frac{tV_b \mu_e \Delta n}{l^2 \eta \Phi_s} \tag{8}$$

and by invoking Eq. (7) we get for the photoconductive gain

$$g = \frac{\tau \mu_e V_b}{l^2} = \frac{\tau}{l^2/\mu_e V_b} \tag{9}$$

So, the photoconductive gain can be defined as

$$g = \frac{\tau}{t_t} \tag{10}$$

where t_t is the transit time of electrons between ohmic contacts. To obtain the last equation, it was taken into account that the carrier drift velocity is given by

$$v_e = \mu_e E \tag{11-1}$$

and the electric field $E = V_b/l$.

Equation (10) indicates that the photoconductive gain is given by the ratio of free carrier lifetime, τ, to transit time, t_t, between the sample electrodes. Carrier lifetime is a strong function of the semiconductor materials used in the photoresistor. The photoconductive gain can be less than or greater than unity depending upon whether the drift length, $L_d = v_d\tau$, is less than or greater than interelectrode spacing, l. The carrier drift velocities are given by

$$v_e = \mu_e E \quad \text{and} \quad v_h = \mu_h E \tag{11-2}$$

In many semiconductors, the mobility of an electron is greater than that of a hole. At high field strengths E, in excess of approximately 10^5 V/cm, a saturation velocity between 6×10^6 cm/s and 10^7 cm/s is observed. The application of even higher strength fields will not increase a carrier's velocity. In most semiconductors the saturation velocities for both holes and electrons are similar, with the hole generally being slightly slower, and a single value for saturation velocity v_s is used for both carriers. In some semiconductors, such as GaAs, InP, and GaN, the electron drift velocity exhibits a distinct peak for field strengths in the vicinity of 10^4 V/cm. Electron velocities as high as 2×10^7 cm/s are obtainable. Since the velocity of the faster carrier determines the transit time in a photoresistor, high-gain photoresistors are sometimes operated at relatively low voltages.

The value of $L_d > l$ implies that a free charge carrier swept out at one electrode is immediately replaced by injection of an equivalent free charge carrier at the opposite electrode. This corresponds to a photogenerated carrier looping through the circuit many times before recombination. The photoconductive gain of intrinsic photoresistor as large as 10^6 has been measured.

When $R_L \gg R$, a signal voltage across the load resistor is essentially the open circuit voltage:

$$V_s = I_{ph} R_d = I_{ph} \frac{1}{qwtn\mu_e} \tag{12}$$

where R_d is the detector resistance. Assuming that the change in conductivity upon irradiation is small compared to the dark conductivity, the voltage responsivity is expressed as

$$R_v = \frac{V_s}{P_\lambda} = \frac{\eta}{lwt} \frac{\lambda\tau}{hc} \frac{V_b}{n_0} \tag{13}$$

where the absorbed monochromatic power $P_\lambda = \Phi_s A h\nu$.

Another figure of merit is the current resposivity, which is the ratio of the photocurrent to the absorbed power. Taking into account Eq. (3) we have

$$R_i = \frac{I_{ph}}{P_\lambda} = \frac{\eta q}{h\nu} g = \frac{\lambda\eta}{hc} qg \tag{14}$$

Therefore, for a given quantum efficiency, both voltage and current resposivities increase linearly with wavelength.

Equation (13) shows clearly the basic requirements for high photoconductive responsivity at a given wavelength λ: One must have high quantum efficiency η, long excess carrier lifetime τ, the smallest possible piece of crystal, low thermal equilibrium carrier concentrations n_0, and the highest possible bias voltage V_b.

The frequency-dependent responsivity can be determined by the equation

$$R_v = \frac{\eta}{lwt} \frac{\lambda\tau_{ef}}{hc} \frac{V_b}{n_0} \frac{1}{(1+\omega^2\tau_{ef}^2)^{1/2}} \tag{15}$$

where τ_{ef} is the effective carrier lifetime. Usually, the photoconductors fabricated from wide bandgap materials reveal strongly sublinear responses, and excitation-dependent response time is observed even at relatively low excitation levels. This can be attributed to the redistribution of the charge carriers with increased excitation level.

The above simple model takes no account of additional limitations related to the practical conditions of photoconductor operation such as sweep-out effects or surface recombination. These are specified below.

Equation (15) shows that voltage responsivity increases monotonically with the increase of bias voltage. However, there are two limits on applied bias voltage, namely, thermal conditions (Joule heating of the detector element) and sweep-out of minority carriers. The thermal conductance of the detector depends on the device fabrication procedure. If the excess carrier lifetime is long, we cannot ignore the effects of

contacts and of drift and diffusion on the device performance. Present-day material technology is such that at moderate bias fields, minority carriers can drift to the ohmic contacts in a time short compared to the recombination time in the material. Removal of carriers at an ohmic contact in this way is referred to as "sweep-out." Minority carrier sweep-out limits the maximum applied voltage of V_b. The effective carrier lifetime can be reduced considerably in detectors where the minority carrier diffusion length exceeds the detector length. At low bias the average drift length of the minority carriers is very much less than the detector length, l, and the minority carrier lifetime is determined by the bulk recombination modified by diffusion to surface and contacts. The carrier densities are uniform along the length of the detector. At higher values of the applied field, the drift length of the minority carriers is comparable to or greater than l. Some of the excess minority carriers are lost at an electrode, and to maintain space charge equilibrium, a drop in excess majority carrier density is necessary. This way the majority carrier lifetime is reduced. It should be pointed out that the loss of the majority carriers at one ohmic contact is replenished by injection at the other, but the minority carriers are not replaced. At high bias the excess carrier density is nonuniformly distributed along the length of the sample.

To achieve high photoelectric gain, low resistance and low surface recombination velocity contacts are required. The metallic contacts are usually far from expectation. The contacts are characterized by a recombination velocity which can be varied from infinity (ohmic contacts) to zero (perfectly blocking contacts). In the latter case, a more intensely doped region at the contact (e.g., n^+ for n-type devices or heterojunction contact) causes a built-in electric field that repels minority carriers, thereby reducing recombination and increasing the effective lifetime and the responsivity.

NOISE MECHANISMS IN PHOTORESISTORS

All detectors are limited in the minimum radiant power which they can detect by some form of noise which may arise in the detector itself, in the radiant energy to which the detector responds, or in the electronic system following the detector. Careful electronic design, including low noise amplification, can reduce the system noise below that in the output of the detector. This topic will not be treated here.

We can distinguish two groups of noise: the radiation noise and the noise internal to the detector. The radiation noise includes signal fluctuation noise and background fluctuation noise. Under most operating conditions the signal fluctuation limit is operative for ultraviolet and visible detectors.

The random processes occurring in semiconductors give rise to internal noise in detectors even in the absence of illumination. There are two fundamental processes responsible for the noise: fluctuations in the velocities of free carriers due to their random thermal motion, and fluctuations in the densities of free carriers due to randomness in the rates of thermal generation and recombination (3).

Johnson–Nyquist noise (the thermal noise) is associated with the finite resistance R of the device. This type of noise is due to the random thermal motion of charge carriers in the crystal and not due to fluctuations in the total number of these charge carriers. It occurs in the absence of external bias as a fluctuating voltage or current depending upon the method of measurement. Small changes in the voltage or current at the terminals of the device are due to the random arrival of charge at the terminals. The root mean square (rms) of the Johnson–Nyquist noise voltage in the bandwidth Δf is given by

$$V_{\mathrm{j}} = (4kTR\Delta f)^{1/2} \tag{16}$$

where k is Boltzmann's constant and T is the temperature. This type of noise has a "white" frequency distribution.

At finite bias currents, the carrier density fluctuations cause resistance variations, which are observed as noise exceeding Johnson–Nyquist noise. This type of excess noise in photoconductive detectors is referred to as generation–recombination (g–r) noise; g–r noise is due to the random generation of free charge carriers by the crystal vibrations and their subsequent random recombination. Because of the randomness of the generation and recombination processes, it is unlikely that there will be exactly the same number of charge carriers in the free state at succeeding instances of time. This leads to conductivity changes that will be reflected as fluctuations in current flow through the crystal. Many forms of g–r noise expression exist, depending upon the internal properties of the semiconductors.

The rms g–r noise current for an extrinsic n-type photoconductor with carrier lifetime τ can be written as

$$I_{\mathrm{g-r}}^2 = \frac{4I^2\overline{\Delta N^2}\tau\Delta f}{(N^2(1+\omega^2\tau^2)} \tag{17}$$

where N is the number of carriers in the detector (3). Usually, in an extrinsic semiconductor there will be some counterdoping—that is, electrons trapped at deep lying levels. If the number of deep traps is small compared to the number of electrons (electrons being the majority carriers), then the variance ΔN^2 is equal to N.[3] The current flowing in the device is $I = Nqg/\tau$, hence

$$I_{\mathrm{g-r}}^2 = \frac{4qIg\Delta f}{1+\omega^2\tau^2} \tag{18}$$

Generation–recombination noise usually dominates the noise spectrum of photoresistors at intermediate frequencies.

An additional type of noise, referred to as 1/f noise, because it exhibits an approximately $1/f$ power law spectrum, is always observed. It is less understood than the more fundamental noise sources and is not generally amenable to mathematical analysis. The general expression for the $1/f$ noise current is

$$I_{1/f} = \left(\frac{KI_{\mathrm{b}}^{\alpha}\Delta f}{f^{\beta}}\right)^{1/2} \tag{19}$$

where K is a proportionality factor, I_b is the bias current, α is a constant whose value is about 2, and β is a constant whose value is about unity.

In general, $1/f$ noise appears to be associated with the presence of potential barriers at the contacts, surface trapping phenomena, and surface leakage currents. Reduction of $1/f$ noise to an acceptable level is an art which depends greatly on the processes employed in preparing the contacts

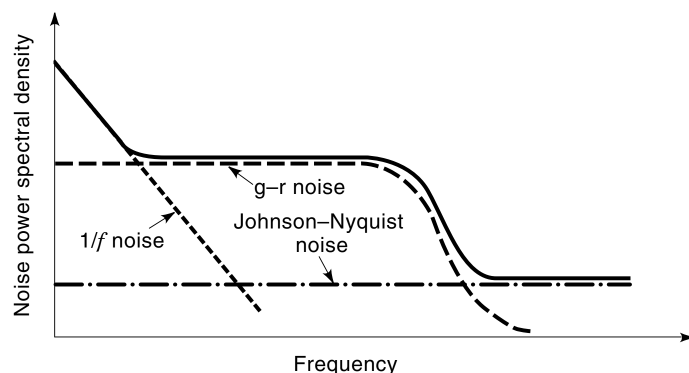

Figure 3. Photoresistor typical noise spectrum.

and surfaces. Up until now, no fully satisfactory general theory has been formulated. The two most current models for the explanation of $1/f$ noise were considered: Hooge's model (4), which assumes fluctuations in the mobility of free charge carriers, and McWhorter's model (3), based on the idea that the free carrier density fluctuates.

The total noise voltage is

$$V_n = (V_j^2 + V_{g-r}^2 + V_{1/f}^2 + V_{pa}^2)^{1/2} \quad (20)$$

Normally, the preamplifier is carefully chosen such that its noise, V_{pa}, is negligible compared to the other sources of noise.

Typical noise-power spectral density of photoresistors is plotted in Fig. 3. The dominant noise at low frequencies is $1/f$ noise, and at mid-frequencies it is g–r noise. The g–r noise rolloff results from the carrier lifetime [see Eq. (17)]. At high frequencies, the g–r noise has fallen off, and the Johnson–Nyquist noise is dominant.

Figure 4 shows a high-frequency equivalent circuit for a photoresistor. The conductance G consists of the dark conductance due to the dark current and the conductance induced by the average signal current and the background current. Two noise current sources are included: the thermal noise and the g–r noise.

QUANTUM EFFICIENCY

A signal whose photon energy is sufficient to generate photocarriers will continuously lose energy to the semiconductor crystal lattice as the optical field propagates through the semiconductor. As illustrated in Fig. 5, at the air-to-semiconductor interface there is a reflection loss due to difference in index of refraction. For many semiconductors used in the visible and infrared region, the reflectivity can be as high as 30%.

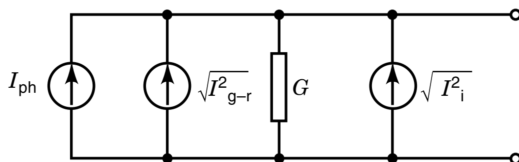

Figure 4. Equivalent circuit of a photoresistor.

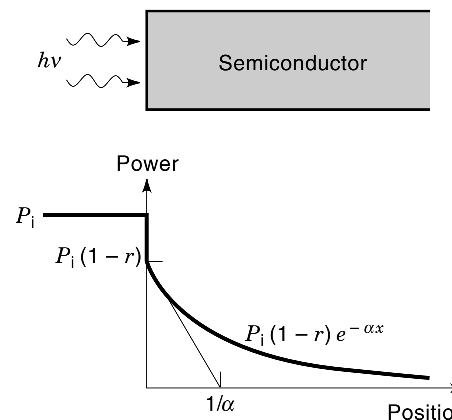

Figure 5. Optical absorption in a semiconductor.

Reflection losses can be reduced with antireflection coatings to less than 1%.

Inside the semiconductor, the field decays away exponentially as energy is transferred to the semiconductor. The material can be characterized by an absorption coefficient α and a penetration depth $1/\alpha$. Penetration depth is a point at which $1/e$ of the optical signal power remains.

The power in the optical field decays with distance. The amount of power absorbed in the semiconductor as a function of position within the material is then

$$P_a(x) = P_i(1-r)(1-e^{-\alpha x}) \quad (21)$$

where P_i is the incident power and r is the reflectivity of semiconductor.

The number of photons absorbed is the power in watts divided by the photon energy $E = h\nu$. The number of photocarriers generated per number of incident photons is just quantum efficiency

$$\eta(x) = (1-r)(1-e^{-\alpha x}) \quad (22)$$

where $0 \leq \eta(x) \leq 1$.

For a photoresistor to have a high quantum efficiency, the surface reflection must be low and the length of the absorbing region must be at least one absorption length long. A long absorption region also implies that carriers will take more time reaching the external circuitry, which will tend to reduce the bandwidth of the photoresistor. There is an inherent tradeoff between our desire to make the absorption region to guarantee that all photons are absorbed and our desire to minimize the time between photocarrier generation and our ability to sense the resulting current.

The absorption length is determined by the absorption coefficient. Figure 6 and 7 show the measured intrinsic absorption coefficients for various photodetector materials. The absorption coefficient and corresponding penetration depth vary among the semiconductor materials. Since α is a strong function of the wavelength, for a given semiconductor the wavelength range in which appreciate photocurrent can be generated is limited. For wavelengths longer than λ_c, the values of α are too small to give appreciable absorption.

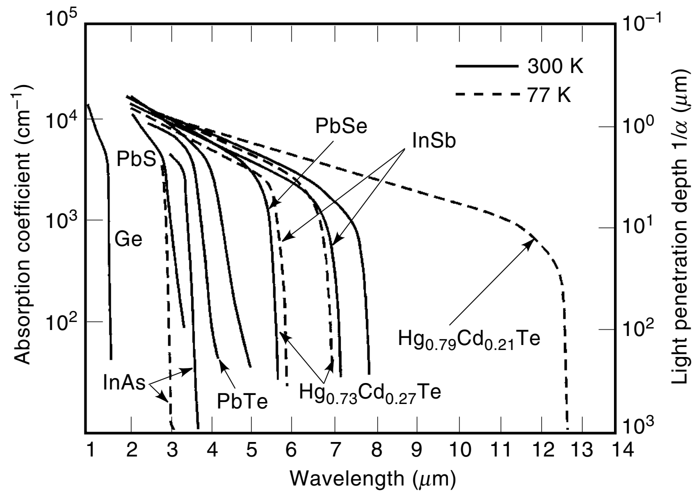

Figure 6. Absorption coefficient for various photodetector materials.

In the case of extrinsic photoresistors the absorption coefficient is

$$\alpha(\lambda) = \sigma_{\mathrm{i}}(\lambda)N_{\mathrm{I}} \tag{23}$$

where $\sigma_i(\lambda)$ is the photoionization cross section and N_I is the neutral impurity concentration.

It would appear desirable to increase N_I without limit to maximize the quantum efficiency, but upper limits to increase the impurity concentration arise from two sources. First, there is a limit to the solubility of the impurity atoms in the semiconductor crystal. These limits range from $\sim 10^{18}$ cm^{-3} to $\sim 10^{21}$ cm^{-3} for commonly used dopants. Secondary, before the solubility limit is reached, the electrical properties of the crystal usually undergo unwanted changes in the form of conductivity modes that cannot be adequately controlled either by operating the detector at low temperatures to freeze out or by other means (e.g., hopping). Given these limitations, typical acceptable impurity concentrations are around 10^{15} cm^{-3} to 10^{16} cm^{-3} for silicon and somewhat lower for germanium.

Practical values of α for extrinsic photoresistors are considerably lower than that of intrinsic photoresistors and are in the range 1 cm^{-1} to 10 cm^{-1} for Ge and 10 cm^{-1} to 50 cm^{-1} for Si. Thus, to maximize quantum efficiency, the thickness of

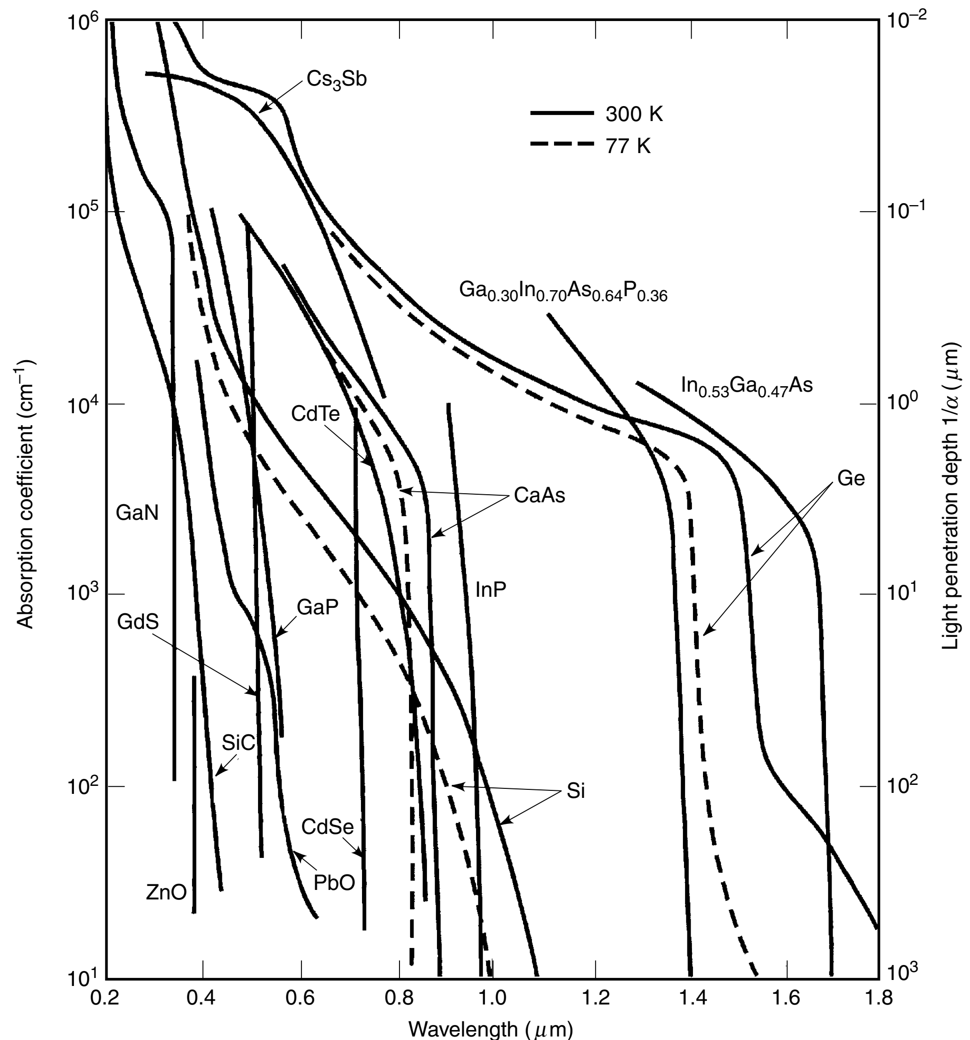

Figure 7. Absorption coefficient for infrared photodetector materials.

the detector crystal should not be less than about 0.5 cm for doped Ge and about 0.1 cm for doped Si. There is a limit in thickness of extrinsic detectors, because photocarriers generated beyond the drift length recombine before being collected. Fortunately, for the most extrinsic detectors the drift length is sufficiently long that quantum efficiencies approaching 50% can be obtained.

PERFORMANCE SPECIFICATION

A relative figure of merit for photodetectors is the noise equivalent power (NEP) that corresponds to the incident rms optical power required to produce a signal-to-noise ratio of 1 in a 1 Hz bandwidth.

The ultimate performance of detectors is reached when the detector and amplifier noise are low compared to the photon noise. The photon noise is fundamental in the sense that it arises not from imperfection in the detector or its associated electronics but rather from the detection process itself, as a result of the discrete nature of the radiation field. The radiation falling on the detector is a composite of that from the target and that from the background.

When photodetectors are operated in conditions where the background flux is less than the optical (signal) flux, the ultimate performance of detectors is determined by the signal fluctuation limit (SFL). It is achieved in practice with photomultipliers operating in the visible and ultraviolet region, but it is rarely achieved with solid-state devices, which are normally detector-noise-limited or electronic-noise-limited. The NEP of detectors operating in this limit have been derived by a number of authors (e.g., see Refs. 5 and 6).

The NEP in the SFL is given by

$$\mathrm{NEP} = \frac{2hc\Delta f}{\eta\lambda} \tag{24}$$

when Poisson statistics are applicable.

The practical operating limit for most infrared detectors is not the signal fluctuation limit but the background fluctuation limit, also known as the background-limited infrared photodetector (BLIP) limit. In this approximation the NEP is given by

$$\mathrm{NEP} = h\nu\left(\frac{2A\Phi_B\Delta f}{\eta}\right)^{1/2} \tag{25}$$

where Φ_B is the total background photon flux density reaching the detector and Δf is the electrical bandwidth of the receiver (5,6). The background photon flux density received by the detector depends on its angular view of the background and on its ability to respond to the wavelengths contained in this source.

For infrared detectors the most frequently used figure of merit is the detectivity, which is defined as

$$D^* = \frac{(A\Delta f)^{1/2}}{\mathrm{NEP}} \tag{26}$$

This parameter can also be defined as

$$D^* = \frac{R_v(A\Delta f)^{1/2}}{V_n} \tag{27}$$

To remove any ambiguity in D^*, one must state whether the radiation is from a black-body source or a monochromatic source and at which modulation frequency. It is recommended that D^* be expressed as $D^*(\lambda, f, l)$ or $D^*(T, f, l)$, where λ is the wavelength in micrometers, f is the frequency of modulation in hertz, T is the blackbody temperature in degrees kelvin, and the reference bandwidth is always in hertz. Detectivity is measured in $\mathrm{cm \cdot Hz^{1/2}\, W^{-1}}$. This unit is also called Jones.

The background limited detectivity of photoresistor is given by

$$D^*_{\mathrm{BLIP}} = \frac{(A\Delta f)^{1/2}}{\mathrm{NEP}} = \frac{\lambda}{2hc}\left(\frac{\eta}{\Phi_B}\right)^{1/2} \tag{28}$$

The temperature of background source varies with ambient conditions, but is typically taken to be 300 K. Plots of D^*_{BLIP} as a function of wavelength for $T_{\mathrm{BLIP}} = 300$ K and for full 2π field of view (FOV) are shown in Fig. 7. The detectivity of BLIP detectors can be improved by reducing the background photon flux, Φ_B. Practically, there are two ways to do this: a cooled or reflective spectral filter to limit the spectral band or a cooled shield to limit the angular FOV of the detector. The former eliminates background radiation from spectral regions in which the detector need not respond. The best detectors yield background-limited detectivities in quite narrow FOVs.

Typical D^* values for available photoresistors are shown in Figs. 8 and 9. Figure 9 shows the spectral detectivity of optical detectors responding in the 0.1 μm to 1.2 μm region. Note that detectivity is not D^*, but rather the reciprocal of NEP for a 1 Hz bandwidth. This figure of merit is employed to include photomultipliers whose noise does not in all cases depend upon the square root of the photocathode area. The reader can convert to the D^* values appropriate to the photoresistors and photovoltaic detectors by multiplying the detectivity value illustrated by the square root of the detector area. The signal fluctuation limit shown in the figure is independent of area [see Eq. (24)].

The photoresistors exhibit the important advantage of the internal photoconductive gain, which relaxes requirements to a low-noise preamplifier. The advantages of p–n junction detectors relative to photoresistors are: low- or zero-bias currents; high impedance, which aids coupling to readout circuits in focal plane arrays; capability for high-frequency operation; and the compatibility of the fabrication technology with planar-processing techniques. In comparison with Schottky barriers, the p–n junction photodiodes indicate also some important advantages. The thermionic emission process in Schottky barriers is much more efficient than the diffusion process, and therefore for a given built-in voltage the saturation current in a Schottky diode is several orders of magnitude higher than that in the p–n junction. In addition, the built-in voltage of a Schottky diode is smaller than that of a p–n junction with the same semiconductor. However, high-frequency operation of p–n junction photodiodes is limited by the minority-carrier storage problem. In other words, the minimum time required to dissipate the carriers injected by the forward bias is dictated by the recombination lifetime. In a Schottky barrier, electrons are injected from the semiconductor into the metal under forward bias if the semiconductor is n-type. Next they thermalize very rapidly ($\sim 10^{-14}$ s) by carrier–carrier colli-

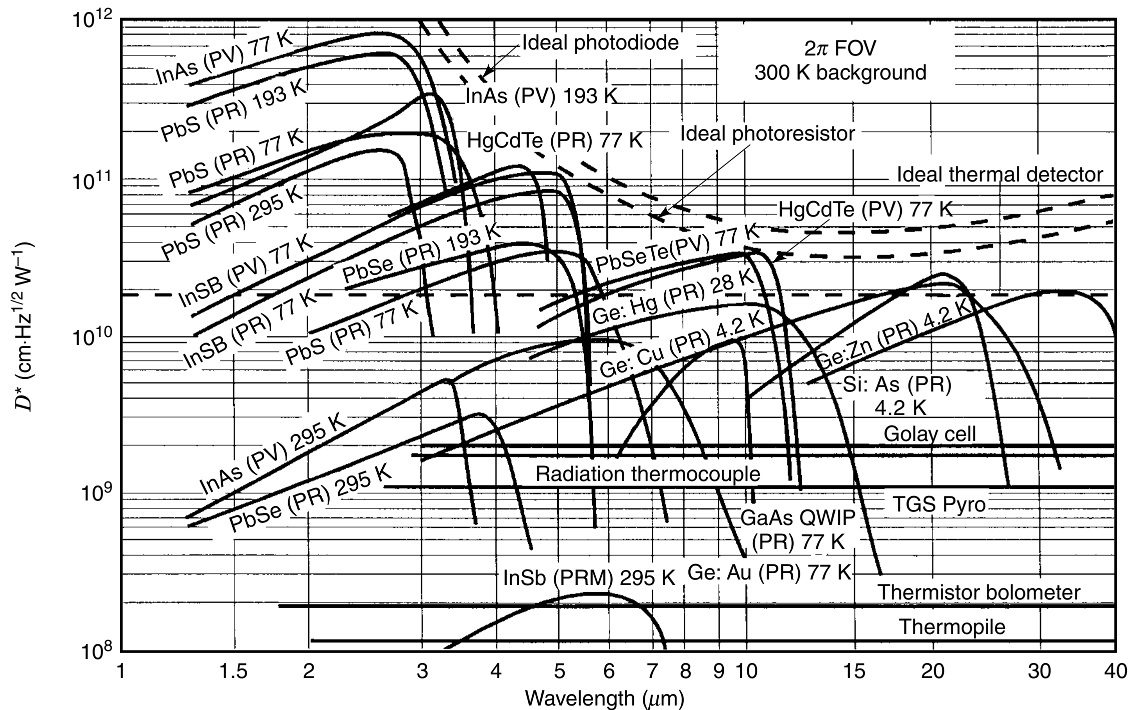

Figure 8. Comparison of the D^* of various commercially available infrared detectors when operated at the indicated temperature. Chopping frequency is 1000 Hz for all detectors except the thermopile (10 Hz), thermocouple (10 Hz), thermistor bolometer (10 Hz), Golay cell (10 Hz), and pyroelectric detector (10 Hz). Each detector is assumed to view a hemispherical surround at a temperature of 300 K. Theoretical curves for the background-limited D^* for ideal photovoltaic (PV) detectors, photoresistors (PR), and thermal detectors are also shown. (After Ref. 7, with permission.)

sions, and this amount of time is negligible compared to the minority-carrier recombination lifetime.

Note that for mid-infrared to far-infrared wavelengths the photoresistors are cooled to lower temperature (see Fig. 10). The lower temperatures reduce thermal effect and increase the photoconductive gain and detection efficiency. For low-level detection at microwave frequencies, however, a photodiode will provide more speed and considerably higher signal-to-noise ratio. Thus photoresistors have limited use in high-frequency optical demodulators, such as in optical mixing. They were, however, extensively used for infrared detectors. Recently, more interest has been focused on p–n junction photodiodes for use with silicon charge-coupled devices (CCDs) in hybrid focal plane arrays for direct detection in the 3 μm to 5 μm and 8 μm to 14μm spectral regions (7). In this application, photodiodes are preferred over photoresistors because of their relatively high impedance, matched directly into the input stage of a silicon CCD, and lower power dissipation.

Note that as carrier lifetime increases, the bandwidth decreases. This is the opposite of what occurred with photoconductive gain, where an increase in carrier lifetime was beneficial. This allows us to draw an important conclusion. Photoconductive gain cannot be increased arbitrarily by increasing carrier lifetime because there is an inherent gain–bandwidth limitation. Given this constraint, one way to achieve high performance is to first engineer the semiconductor so that the carrier lifetime is as long as possible while still maintaining adequate bandwidth. The photoconductive gain is then increased by decreasing the transit time as much as possible. Transit time is then minimized by keeping the path between the electrodes short. The interdigitated electrode structure illustrated in Fig. 10 is a popular technique for reducing transit time while maintaining adequate carrier lifetime and responsivity. The electrodes can also be made optically transparent, further increasing responsivity. Interdigitated photoresistors based on InGaAs have been fabricated with gains of 50 to 100 and bandwidths of a few gigahertz. Silicon-based photoresistors have been demonstrated with gains as high as 1000. The bandwidth in these high-gain devices is lower, typically a few megahertz maximum.

PRACTICAL APPLICATIONS OF PHOTORESISTORS

Photoresistors fabricated from high-resistivity semiconductors are used to detect ultraviolet, visible, and infrared radiation. Wide-bandgap photoresistors such as CdS and CdSe are mainly used in the near-ultraviolet to visible spectral region. Both detectors have a spectral responsivity similar to that of the human eye. Photoresistors can serve as optical switches, which usually require illumination of the entire sensitive region between the electrodes. Linear position sensing, however, does not require the entire photoresistor to be illuminated. By comparing the signals between the electrodes and a third contact, the centroid of incident beam can be determined.

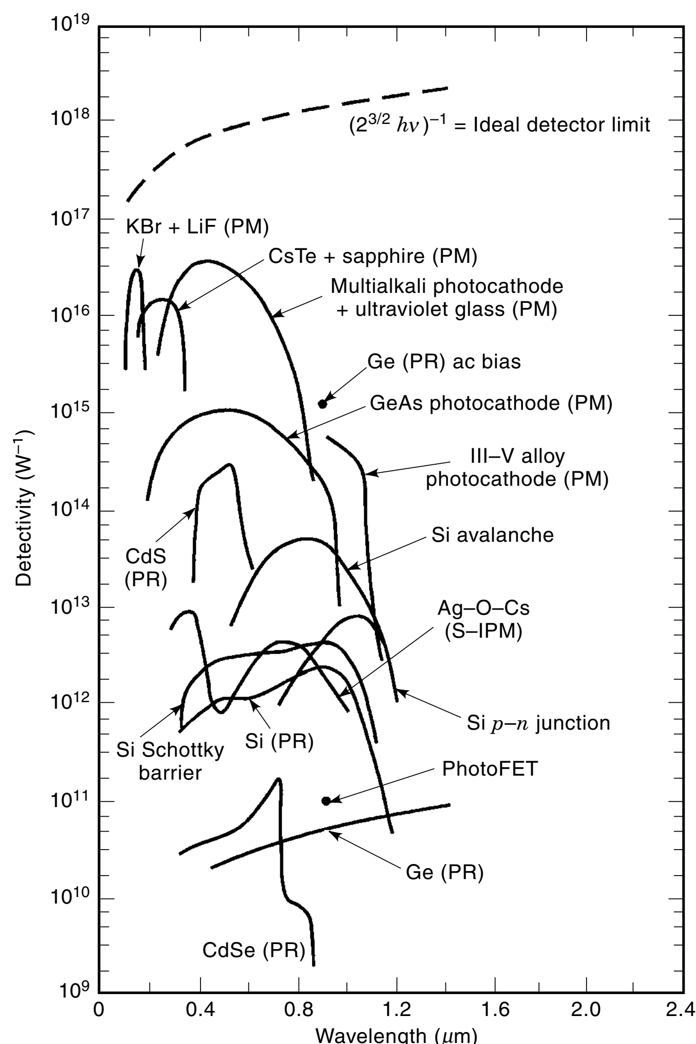

Figure 9. Detectivity versus wavelength values of 0.1 μm to 1.2 μm photodetectors. PR indicates a photoresistors and PM indicates a photomultiplies. Detector areas are given in Table 3 (After Ref. 8, with permission.)

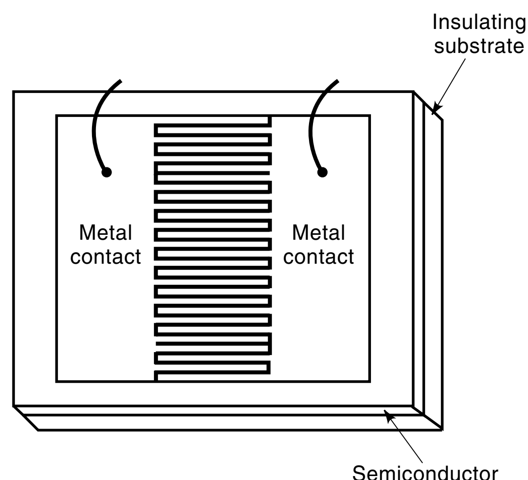

Figure 10. Photoresistor with an interdigitated electrode structure.

Different semiconductor compounds have been used to fabricate photodetectors with spectral responses in the ultraviolet region. Historically, the development of a high-quantum-efficiency semiconductor detector in the whole ultraviolet range has been hampered by the extremely strong absorption and strong radiation-induced aging effects in most of the semiconductor materials. It is especially visible in the case of silicon. For this semiconductor the photon penetration depth ranges from less than 10 nm in the near-ultraviolet and mid-ultraviolet to 100 μm for 10 keV X rays. Development of high-quality III–V nitride semiconductor layers (mainly AlGaN ternary alloy) in the last several years has resulted in the fabrication of a new generation of ultraviolet detectors (9). Due to their wide bandgap, the III–V nitrides are expected to exhibit superior radiation hardness characteristics compared to Si.

Narrow-bandgap photoresistors are used in infrared spectral region. Intrinsic detectors such as lead sulfide (PbS), lead selenide (PbSe), indium antimonide (InSb), and mercury cadmium telluride (HgCdTe), usually operating at temperature below 200 K, are used for 3 μm to 5 μm infrared detection. For longer wavelengths (i.e., $\lambda > 8$ μm), prevailing position is occupied by HgCdTe. At present, HgCdTe as the most important intrinsic semiconductor alloy systems for infrared detectors is well established (7). The specific advantages of HgCdTe are the direct energy gap, ability to obtain both low and high carrier concentrations, high mobility of electrons, and low dielectric constant. HgCdTe can be used for detectors operated at various modes, and it can be optimized for operation at the extremely wide range of the infrared spectrum (1 μm to 30 μm) and at temperatures ranging from that of liquid helium to room temperature. The operating temperature for HgCdTe detectors is higher than that for other types of photon detectors. HgCdTe detectors with background limited performance operate with thermoelectric coolers in the medium wavelength range (3 μm to 5 μm), while the long wavelength detectors (8 μm to 14 μm) operate at ~100 K.

Extrinsic photoresistors are used in a wide range of the infrared spectrum extending from a few micrometers to approximately 300 μm. They are the principal detectors operating in the range $\lambda > 20$ μm. Detectors based on silicon and germanium have found the widest application as compared with extrinsic photodetectors on other materials. Si has several advantages over Ge; for example, three orders of magnitude higher impurity solubilities are attainable, hence thinner detectors with better spatial resolution can be fabricated from silicon. Si has lower dielectric constant than Ge, and the related device technology of Si has now been more thoroughly developed, including contacting methods, surface passivation, and mature metal-oxide semiconductor (MOS) and CCD technologies. Moreover, Si detectors are characterized by superior hardness in nuclear radiation environments.

The availability of a highly developed silicon MOS technology facilitates the integration of large detector arrays with charge-transfer devices for readout and signal processing. The well-established technology also helps in the manufacturing of uniform detector arrays and the formation of low-noise contacts. Although the potential of large extrinsic silicon focal plane arrays for terrestrial applications has been examined, interest has declined in favor of HgCdTe and InSb with their more convenient operating temperatures. Strong interest in doped silicon continues for space applications, particularly in

low background flux and for wavelengths from 13 μm to 20 μm, where compositional control is difficult for HgCdTe. The shallower impurity energies in germanium allow detectors with spectral response up to beyond 100 μm wavelength, and major interest still exists in extrinsic germanium for wavelengths beyond about 20 μm.

It should be noted that in the last 10 years, considerable progress in long-wavelength infrared detectors has been achieved using a new class of solid-state materials, which can be obtained by assembling multilayer structures in which two components alternate in very thin films. Among different types of quantum well infrared photodetectors (QWIPs), technology of the GaAs/AlGaAs multiple quantum well photoresistors is the most mature (10).

SPRITE DETECTORS

The SPRITE (Signal PRocessing In The Element) detector is a new type of photoresistor for use in scanned thermal imaging systems. It was originally invented by T. C. Elliott and developed further almost exclusively by British workers (11). The important benefit that this device achieves is that the time delay and integration (TDI) required in serial scan thermal imaging systems is performed within a single detector element. In a conventional serial scan system the image of the scene is scanned across a series of discrete detectors, the output for each device is then amplified and delayed by the correct amount so that all the detector outputs can be integrated in phase. In the SPRITE detectors these functions are actually performed in the element.

The operating principle of the SPRITE detector is shown in Fig. 11. The device is essentially an ~1-mm-long, 62.5-μm-wide, and 10-μm-thick n-type photoresistor with two bias contacts and a readout potential probe. The device is constant-current-biased, with the bias field E set such that the ambipolar drift velocity v_a, which approximates to the minority hole drift velocity v_d, is equal to the image scan velocity v_s along the device. These conditions are fulfilled for HgCdTe, and the SPRITE detectors are fabricated only from this material. The length of the device, L, is typically close to or larger than the drift length $v_d\tau$, where τ is the recombination time. Consider now an element of the image scanned along the device. The excess carrier concentration in the material increases during scan, as illustrated in Fig. 11. When the illuminated region enters the readout zone, the increased conductivity modulates the output contacts and provides an output signal. Thus the signal integration—which, for a conventional array, is done by external delay line and summation circuitry—is done in the SPRITE detector in the element itself.

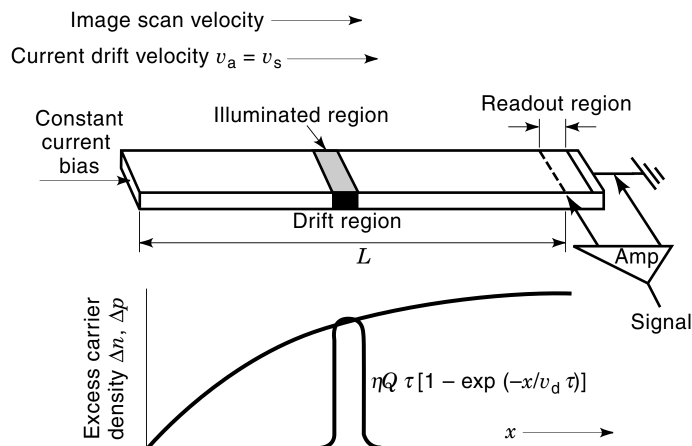

Figure 11. The operating principle of a SPRITE detector. The upper part of the figure shows a HgCdTe filament with three ohmic contacts. The lower part shows that the buildup of excess-carrier density in the device as a point in the image is scanned along it (After Ref. 11, with permission.)

The integration time approximates the recombination time τ for long devices. It becomes much longer than the dwell time τ_{pixel} on a conventional element in a fast-scanned serial system. Thus, a proportionally larger ($\propto \tau/\tau_{pixel}$) output signal is observed. When Johnson noise or amplifier noise dominates, this leads to a proportional increase in the signal-to-noise ratio with respect to a discrete element. In the background-limited detector, the excess carrier concentration due to background also increases by the same factor, but corresponding noise is proportional only to integrated flux. As a result the net gain in the signal-to-noise ratio with respect to a discrete element is increased by a factor $(\tau/\tau_{pixel})^{1/2}$.

It can be shown (11) that the detectivity of a SPRITE detector is equal given by

$$D^* = (2\eta)^{1/2} D^*_{BLIP} \left(\frac{1}{w}\right)^{1/2} \left(\frac{\tau}{\tau_a}\right)^{1/2} \tag{29}$$

which is equivalent to

$$D^* = (2\eta)^{1/2} D^*_{BLIP} (s\tau)^{1/2} \tag{30}$$

From the above equations we see that long lifetimes are required to achieve large gains in the signal-to-noise ratio. Useful improvement in detectivity relative to a BLIP-limited discrete device D^*_{BLIP} can be achieved when the value of $s\tau$ exceeds unity. The performance of the device can be described in terms of the number of BLIP-limited elements in a serial array giving the same signal-to-noise ratio,

$$N_{eq}(\text{BLIP}) = 2s\tau \tag{31}$$

For example, a 60-μm-wide element scanned at a speed of 2×10^4 cm/s and with τ equal to 2 μs gives N_{eq}(BLIP) = 13.

The performance achieved in the 3 μm to 5 μm band is illustrated in Fig. 12. The detectivity increases with the bias field except at the higher fields where the element temperature is raised by Joule heating. Useful performance in this band can be obtained at temperatures up to about 240 K.

The SPRITE detectors are fabricated from lightly doped (~5×10^{14} cm^{-3}) n-type HgCdTe. Single and 2-, 4-, 8-, 16-, and 24-element arrays have been demonstrated; the 8-element arrays are the most common at present (Fig. 13). In order to manufacture the devices in line, it is necessary to reduce the width of the readout zone and corresponding contacts to bring them out parallel to the length of the element within the width of the element as shown in Fig. 13. Various modifications of the device geometry have been proposed to improve both the detectivity and spatial resolution. The modifications have included horn geometry of the readout zone to reduce the transit time spread and slight taper of the drift

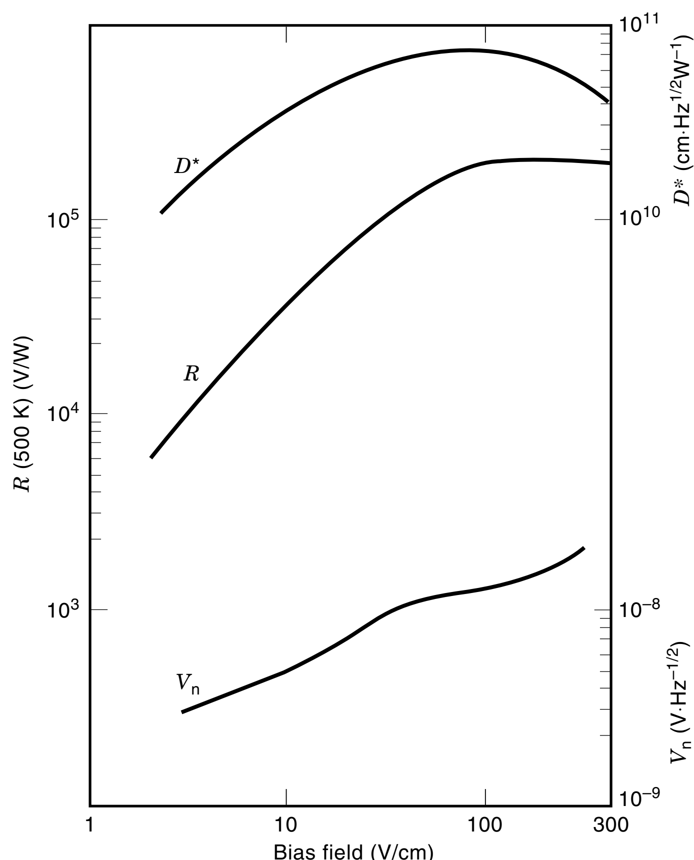

Figure 12. Performance of a 3 μm to 5 μm SPRITE operating at 190 K. (After Refs. 11 and 12, with permission.)

region to compensate a slight change of drift velocity due to background radiation.

Despite remarkable successes, SPRITE detectors have important limitations such as limited size, stringent cooling requirements, and the necessity to use fast mechanical scanning. The ultimate size of SPRITE arrays is limited by the significant heat load imposed by Joule heating.

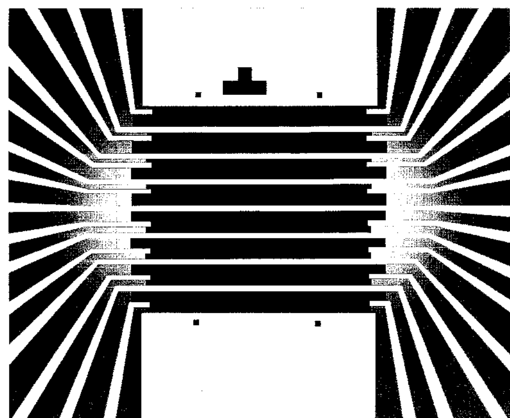

Figure 13. Schematic of an eight-row SPRITE array with bifurcated readout zones. (After Ref. 12, with permission.)

BIBLIOGRAPHY

1. R. A. Smith, *Semiconductors,* Cambridge, UK: Cambridge Univ. Press, 1978.
2. E. S. Rittner, Electron processes in photoconductors, in R. G. Breckenbridge, B. Russel, and E. Hahn (eds.), *Photoconductivity Conf. Atlantic City 1954,* New York: Wiley, 1956, pp. 215–268.
3. A. Van der Ziel, *Fluctuation Phenomena in Semiconductors,* London: Butterworths, 1959.
4. F. N. Hooge, 1/*f* noise is no surface effect, *Phys. Lett.,* **29A**: 123–140, 1969.
5. P. W. Kruse, L. D. McGlauchlin, and R. B. McQuistan, *Elements of Infrared Technology,* New York: Wiley, 1962.
6. P. W. Kruse, The photon detection process, in R. J. Keyes (ed.), *Optical and Infrared Detectors,* Berlin: Springer-Verlag, 1977, pp. 5–69.
7. A. Rogalski (ed.), *Infrared Photon Detectors,* Bellingham, WA: SPIE Optical Engineering Press, 1995.
8. D. H. Seib and L. W. Aukerman, Photodetectors for the 0.1 to 1.0 μm spectral region, in L. Morton (ed.), *Advances in Electronics and Electron Physics,* Vol. 34, New York: Academic Press, 1973, pp. 95–221.
9. M. Razeghi and A. Rogalski, Semiconductor ultraviolet detectors, *J. Appl. Phys.,* **79**: 7433–7473, 1996.
10. B. F. Levine, Quantum-well infrared photodetectors, *J. Appl. Phys.,* **74**: R1–R81, 1993.
11. C. T. Elliott, Infrared detectors with integrated signal processing, in *Solid State Devices,* in A. Goetzberger and M. Zerbst (eds.), Weinheim: Verlag Chemie, 1983, pp. 175–201.
12. A. Blackburn et al., The practical realization and performance of SPRITE detectors, *Infrared Phys.,* **22** (1): 57–64, 1982.

MANIJEH RAZEGHI
Northwestern University

ANTONI ROGALSKI
Military University of Technology

PHOTOSYNTHESIS. See SOLAR ENERGY CONVERSION.